THE ASTROPHYSICAL JOURNAL, 455:300–316, 1995 December 10

A STUDY OF THE CHROMOSPHERICALLY ACTIVE, SHORT-PERIOD BINARY VZ PISCIUM

BRUCE J. HRIVNAK[1,2]
Department of Physics and Astronomy, Valparaiso University, Valparaiso, IN 46383; bhrivnak@exodus.valpo.edu
EDWARD F. GUINAN[1]
Department of Astronomy and Astrophysics, Villanova University, Villanova, PA 19085; guinan@ucis.vill.edu
AND
WENXIAN LU[3]
Department of Physics and Astronomy, Valparaiso University, Valparaiso, IN 46383; wlu@kepler.valpo.edu
Received 1994 December 27; accepted 1995 June 6

ABSTRACT

The short-period binary VZ Piscium is unusual in that it has a high space velocity, indicating that it is old, and a high mass ratio, suggesting that it is presently evolving into contact with little mass exchange having occurred between the components. In this study, we obtained *IUE* and visible spectra to investigate Mg II h+k and Ca II H and K emission strengths. Both features are found to be strong and variable. From the visible spectra, radial velocities were measured, and a new mass ratio of $q = 0.80$ was determined. This mass ratio was used in a new light-curve analysis, and the system was found to be in marginal contact, with the secondary component slightly detached. A model with bright (hot) regions on the inner hemisphere of the slightly detached, less massive component was found to fit well with the variety of spectroscopic and photometric observations of the system. The masses determined for the components are compatible with normal K dwarfs.

Subject headings: binaries: eclipsing — stars: individual (VZ Piscium)

1. INTRODUCTION

VZ Piscium (BD +04°5012; G29–37) is a 10th magnitude, short-period ($0^d.261$) binary system with late-type (K2–5) components. It has a large space motion ($S = 120$ km s^{-1} relative to the local standard of rest) and an ultraviolet excess, indicating that it is an old disk population star with a kinematic age of $8 < T < 10$ Gyr (see Eggen 1967; Hrivnak & Milone 1989; Guinan & Bradstreet 1988). VZ Psc also displays exceptionally strong Ca II H and K emission lines in its optical spectrum (Wolff, Wallerstein, Sandage 1965), indicating high levels of chromospheric activity and inferred high levels of magnetic activity.

Light curves of VZ Psc have been obtained by Eggen (1967), Bradstreet (1985), Davidge & Milone (1984), Milone et al. (1985), and Samec (1989). These light curves show a low-amplitude light variation, primarily arising from the distorted shapes of the tidally interacting stars. One unusual aspect of the recent light curves is that the primary and secondary minima have significantly different depths. This is not true of the initial light curve of Eggen (1967), which showed minima of similar depths and appeared to be that of a low-amplitude W Ursae Majoris binary. Thus, the light curve of the system has changed from that of W UMa type, with continuous light variation and minima of nearly equal depths, to a Beta Lyrae type, with continuous light variation but minima of unequal depths. The system also displays intrinsic variability of its light curve on timescales of weeks to years (see Bradstreet 1985; Samec 1989).

Radial velocity curves have been obtained by Hrivnak & Milone (1989) using the cross-correlation technique. These yield a mass ratio of $q \sim 0.9$ for the system, a value closer to unity than that reported for any other W UMa or cool contact binary. Most W UMa binaries have a mass ratio q in the range $0.6 > q > 0.2$. The nearly equal masses inferred for the components suggest that the system may have recently evolved into a contact configuration from a previously wider, detached binary by angular momentum loss (AML) via magnetic braking (see, e.g., Vilhu 1982; Hrivnak & Milone 1989; Guinan & Bradstreet 1988).

Analyses of the light curves have been carried out by several investigators, leading to different interpretations of the system and to inconsistencies. The chief difficulty in the light-curve solutions is the low-amplitude nature of the light curve and the minima of unequal depths. Bradstreet (1985), Hrivnak & Milone (1989), and Barone et al. (1989) have analyzed the light curves of VZ Psc, with similar results. These all indicate a greatly overcontact configuration, with large fill-out factors of 56%–95% and with very large temperature differences between components of $\Delta T \sim 800$–1200 K. These solutions also indicate a low orbital inclination $i \sim 33°$–$40°$ with very shallow eclipses or no eclipses at all. The major problem with these solutions is that it is difficult physically to explain a large thermal discontinuity between two stars in such close geometric contact. In addition, the low orbital inclination in these studies, when combined with the radial velocity results, leads to component masses of 1.1–1.3 $M_\odot$, which are about 60% larger than expected for main-sequence K2–K5 stars.

These problems are for the most part resolved by the more recent light-curve analysis carried out by Maceroni, Van Hamme, & van't Veer (1990). They fitted the light curve by assuming that two, nearly stationary, dark starspots are located on the exterior hemisphere of the smaller, less massive star. The spots depress and widen the deeper minimum, producing the difference in the depths of primary and secondary and the apparent temperature discontinuity found in the

[1] Guest Observer, *International Ultraviolet Explorer* satellite.
[2] Visiting Astronomer, Dominion Astrophysical Observatory, Herzberg Institute of Astrophysics.
[3] On leave from Shanghai Observatory, Academia Sinica.

previous studies. In their solution with starspots, the system is marginal undercontact rather than overcontact, and the temperature difference between the stars is reduced to $\Delta T \sim 200$ K. Moreover, with a higher value of $i \sim 49°$, the inferred masses of the stars are compatible with their K2–5 spectral types. The introduction of cool starspots may seem ad hoc, but the strong Ca II H and K emission and rapid rotation of the components imply vigorous magnetic dynamo activity. Furthermore, spots have been inferred from the analysis of light curves of other cool W UMa stars (Binnendijk 1970, 1984; Linnell 1982; Bradstreet & Guinan 1990) and in the RS CVn and BY Dra stars (see, e.g., Rodono et al. 1986; Guinan & Giménez 1993). A puzzling aspect of the spots on VZ Psc is that they would tend to be located preferentially on the back side of the smaller, less massive star.

With the knowledge that the system displayed strong Ca II emission, we decided to investigate the level of the chromospheric activity and search for phase-dependent variability by observing the Mg II (λ2800) and Ca II H and K emission. In this paper, we describe our *IUE* observations, which indicate variability in the Mg II emission feature. We then go on to describe our visible-band spectroscopy, which indicates that the Ca II emission strength also varies. Radial velocities are measured for these spectra, and a new radial velocity solution is determined. The resulting mass ratio is used in a new light-curve solution of the system. The result of this multiwavelength study are then discussed in an effort to arrive at a unified picture of this active, short-period binary.

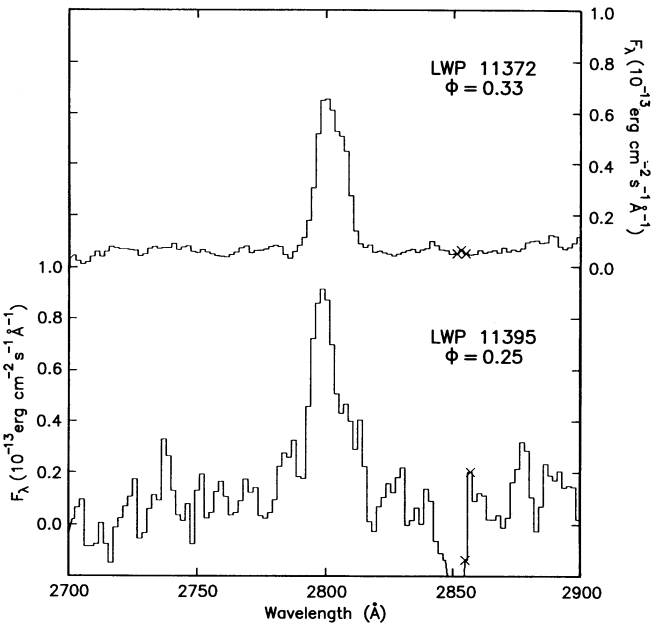

FIG. 1.—Two representative LWP spectra of VZ Psc, both taken near orbital phase 0.3, but 3 days apart. The variation in the strength of the Mg II feature at 2800 Å is evident. Note that due to a higher background radiation level, the exposure time for LWP 11395 is less, 20 minutes versus 45 minutes and the spectrum contains more noise.

2. THE *IUE* OBSERVATIONS

VZ Psc was observed with the *IUE* satellite on 1987 August 11 and 14. Because of its faintness, only the low-dispersion cameras were used, and all observations were made through the large aperture. The long-wavelength primary (LWP) camera (which covers $\lambda\lambda$1900–3200) was used in two US2 shifts to obtain spectra at different orbital aspects, chiefly to search for possible phase-related variations in the emission strength of the Mg II h+k feature at 2800 Å. The exposure times with the LWP were relatively short, ranging from 20 to 45 minutes, with the shorter exposures limited by a high background radiation level. A total of nine LWP spectra were obtained of VZ Psc. Figure 1 shows two representative LWP spectra of VZ Psc obtained near the same orbital phase ($\sim$0.3*P*), but 3 days apart. The Mg II h+k line is very prominent in all these spectra and appears to vary with time and possibly orbital phase. Table 1 gives the observing log of the *IUE* observations made of VZ Psc with the LWP camera. The Heliocentric Julian Date (HJD) refers to the time of midexposure, and the phase is determined from the ephemeris given below in equation (1).

On August 11 a single long exposure (t_{exp} = 380 minutes), which covered the 6^h16^m orbital period of the binary, was obtained with the short-wavelength primary (SWP) camera during the low-radiation US1 shift. This SWP spectrum (SWP 31536) is underexposed but adequate for determining the presence and strengths of strong chromospheric and transition-region emission features commonly found in active cool stars within the $\lambda\lambda$1150–2000 bandpass of the SWP camera. This SWP spectrum is shown in Figure 2, with the stronger emission features identified. The integrated net emission fluxes of the emission features were measured using the standard *IUE*/RDAF procedures and are given in Table 2. These lead to a total transition region flux, summing up the values from N V, Si IV, and C IV, of 11.0×10^{-14} ergs cm^{-2} s^{-1} received at Earth. The value of the bolometric flux used in Table 2 is calculated using the method described below.

TABLE 1

IUE OBSERVING LOG WITH LWP CAMERA FOR VZ PISCIUM

LWP	HJD (2,440,000+)	Phase	Exposure Time (minutes)	f(Mg II)[a] (10^{-13} ergs cm^{-2} s^{-1})	R(Mg II)	f(λ2950)[a] (10^{-13} ergs cm^{-2} s^{-1})
11371.....	7018.6407	0.04	35	6.2	19	9.9
11372.....	7018.9762	0.33	45	8.0	20	12.2
11373.....	7019.0435	0.58	45	9.3	26	15.0
11374.....	7019.1067	0.83	35	7.6	19	13.1
11392.....	7021.9124	0.57	40	7.4	21	11.4
11393.....	7021.9860	0.85	40	7.6	19	12.0
11394.....	7022.0478	0.08	30	7.9	24	12.7:
11395.....	7022.0916	0.25	20	10.8	27	...
11396.....	7022.1305	0.40	20	7.4	19	...

[a] Integrated flux received at Earth.

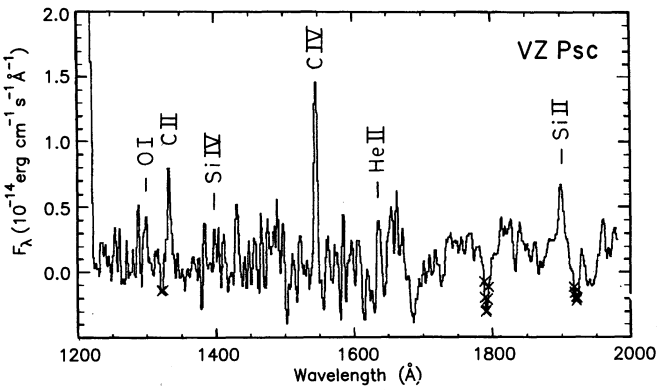

FIG. 2.—The SWP spectrum of VZ Psc, with two-point smoothing. The stronger transition region features are indicated.

In addition to obtaining UV spectra, the fine error sensor (FES) on board the satellite was used to obtain an optical light curve of VZ Psc. To compensate for possible drifts in sensitivity of the FES with time, occasional measurements of a nearby comparison star (or offset star) were made in the same way as those of VZ Psc, and differential magnitudes were determined. For this purpose, SAO 128211 (HD 221235 = BD +04°5061; m_v = 7.3; K0) served as the comparison star for the differential photometry; this is the same comparison star used in some of the ground-based photoelectric studies of the binary. The differential FES measures were corrected for dead time and transformed (approximately) to differential ΔV magnitudes using the calibration of Imhoff & Wasatonic (1986). The FES differential V magnitudes [ΔV(FES)], in the sense of the variable star minus the comparison star, and the corresponding times, converted to Heliocentric Julian Dates (HJD), are listed in Table 3. Phases were computed using the ephemeris from Bradstreet (1985):

Heliocentric Primary Minimum

$$= 2{,}444{,}556.5246 + 0.26125902E\ . \quad (1)$$

The period study of the system indicates no evidence of a period change since the first light curve by Eggen (1967) in 1967 up to the most recently published light curves of 1986 (Samec 1989). We do note the odd circumstance that in the light curve plotted by Eggen, the slightly deeper minimum is plotted at 0.5 phase. If the time of primary minimum quoted by Eggen refers to the slightly shallower minimum plotted at 0.0 phase, then the above period is in need of revision.

TABLE 2

EMISSION-LINE FLUXES FROM THE SWP SPECTRUM (SWP 31536) OF VZ PISCIUM

Line	λ(Å)	Flux at Earth (10^{-14} ergs cm^{-2} s^{-1})	F(line)/F(bol) ($\times 10^6$)
N V	1240	1.20:	3.3
O I+Si III	~1300	2.56	7.0
C II	1335	5.27	14.3
Si IV	1400	2.14	5.8
C IV	1550	7.61	20.7
He II	1640	1.96	5.3

NOTE.—These values lead to a total transition region flux, derived from summing the contributions of N V, Si IV, and C IV, of 11.0 × 10^{-14} ergs cm^{-2} s^{-1}.

TABLE 3

IUE FES LIGHT CURVE OF VZ PISCIUM

HJD (2,440,000+)	Phase	ΔV(FES)
7018.6171.....	0.952	3.05
7018.6220.....	0.971	3.08
7018.6546.....	0.096	3.02
7018.6560.....	0.101	3.02
7018.9286.....	0.144	3.07
7018.9289.....	0.146	3.05
7018.9518.....	0.233	2.96
7018.9525.....	0.236	2.95
7018.9942.....	0.396	3.05
7018.9956.....	0.401	3.06
7019.0227.....	0.505	3.10
7019.0241.....	0.510	3.09
7019.0616.....	0.654	3.00
7019.0623.....	0.656	3.00
7019.0894.....	0.760	2.96
7019.0900.....	0.762	2.95
7019.1289.....	0.911	3.03
7019.1296.....	0.914	3.02
7021.8930.....	0.491	3.06
7021.9293.....	0.630	3.06
7021.9680.....	0.778	2.94
7021.9694.....	0.784	2.94
7022.0020.....	0.908	3.08
7022.0034.....	0.914	3.09
7022.0333.....	0.028	3.17
7022.0340.....	0.031	3.19
7022.0603.....	0.131	3.05
7022.0610.....	0.134	3.04
7022.0812.....	0.211	2.97
7022.0819.....	0.214	2.98
7022.1194.....	0.358	2.96
7022.1201.....	0.360	2.97

The FES light curve is shown in Figure 3. Although only sparsely populated and of lower quality, it resembles in general the recent 1986 light curves of Samec (1989) in having two minima of unequal depths and maxima of slightly different heights. The depths of primary and secondary minima relative to the mean brightness of the two maxima are 0.243 ± 0.018 and 0.145 ± 0.015 mag, respectively. For comparison, Samec's

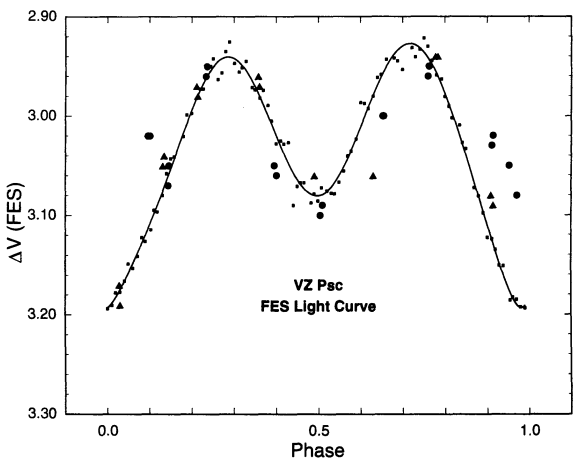

FIG. 3.—The *IUE* V(FES) light curve of VZ Psc, with circles representing the data from 1987 August 11 and triangles representing the data from August 14. For comparison, we also display the V light curve of Samec (1989), with small squares representing normal points and the sold line representing a polynomial fit (ninth-order) to Samec's data.

1986 V light curve yields primary and secondary minima depths of 0.257 ± 0.007 and 0.147 ± 0.006 mag, respectively. We have shown for comparison in Figure 3 the V light curve of Samec, gathered into normal points, and as a solid line a polynomial fit (ninth-order) to Samec's data. In comparison with Samec's light curve, the new FES light curve displays a narrower primary minimum and a wider, deeper secondary minimum. Changes in the light curve of VZ Psc will be discussed in § 4.

The Mg II emission-line fluxes f(Mg II) were measured by integrating the flux above the adjacent spectrum. Because of the weakness of the adjacent continuum for the K2–5 stars of VZ Psc, there was little uncertainty in extracting the f(Mg II) measures. The Mg II emission measures are listed as f(Mg II) in Table 1. The last three observations, made when the radiation background was high and the exposure time short, contain more noise and are less precise. Following the procedure of Rucinski (1985), we next computed the quantity R(Mg II) = f(Mg II)/f(bol), where the bolometric flux f(bol) was determined from the light level of the optical light curve at the phase where the spectrum was made. The value of f(bol) is given by Rucinski (1985) as

$$f(\text{bol}) = 2.7 \times 10^{-5} \text{ dex } [-0.4m(\text{bol})] \text{ ergs cm}^{-2} \text{ s}^{-1}, \quad (2)$$

where m(bol) = V + BC. The value of V was determined from the mean light curve, while the bolometric correction (BC) was estimated on the basis of $(B-V)$ for the system using the tabulation of Johnson (1966). In the case of VZ Psc, $(B-V) = +1.19$ and BC = 0.62 mag. The values of R(Mg II) calculated in this way are listed in Table 1. We estimate the relative uncertainty to be ~5% for the first six values of R(Mg II) and ~15% for the last three, more noisy measurements. The quantity R(Mg II) in principle normalizes the Mg II emission flux to the visible projected surface areas of the stars.

The values of R(Mg II) are plotted against orbital phase in Figure 4. The data from the two different nights are identified with different symbols in the figure. Variations in the Mg II emission are apparent on each night. On 1987 August 11, the value of R(Mg II) appeared to be constant, R(Mg II) ~ 19×10^{-5}, except for one measure near 0.6P, when R(Mg II) ~ 26×10^{-5}. It is not possible to tell from this night's data alone if this enhancement is a phase-dependent change related to the visibility of an active region on one of the stars or is caused by a transient flarelike event. Three days later, the Mg II emission had a different behavior, beginning and ending at a similar lower level of R(Mg II) ~ 20×10^{-5}, but rising to a maximum of R(Mg II) ~ 27×10^{-5} between 0.00 and 0.25 phase. The 1987 August 14 observations indicate that after 0.25 phase, the Mg II emission level was returning to the level it had nearly one orbital cycle earlier. This could indicate a phase-dependent variation at this time in which an active flaring region came into view between 0.85 and 0.08 phase and receded from view after 0.3 phase. Without additional observations, it is impossible to determine whether this enhancement in Mg II emission had a phase-dependent component or whether the observations suggest the characteristic time (~2 hr) of flare events on stars.

To investigate this further, we also measured the continuum in the region 2900–3000 Å, a region where the signal is relatively good and without strong emission features. These values are listed in Table 1, except for the last two spectra, which were taken with the high radiation background and consequently shorter exposure times, and for which the measurements were significantly less reliable. We found that this λ2950 continuum varied in the same way as the Mg II emission. Thus, while the Mg II emission varies and the ratio of Mg II emission to the bolometric flux (based on the V light curve) varies, the ratio of Mg II emission to the ultraviolet continuum (λ2950) is nearly constant.

Comparison of the average value of R(Mg II) for VZ Psc with other W UMa binaries can be made by using the results of Rucinski (1985) and Vilhu & Walter (1987). Figure 5, adopted for Rucinski (1985), shows VZ Psc along with other W UMa stars, plotted in a diagram of R(Mg II) versus $(b-y)$ color. For

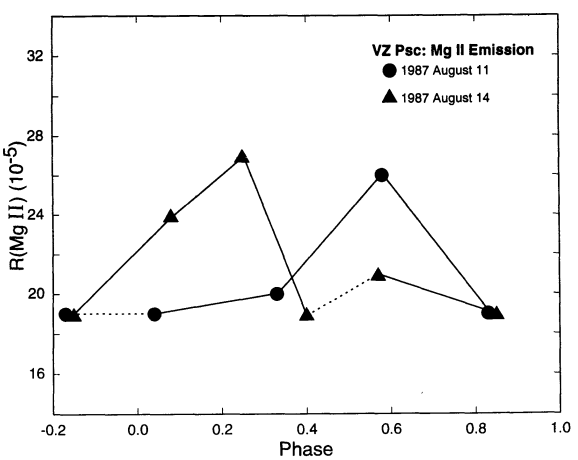

FIG. 4.—Normalized Mg II flux vs. orbital phase for VZ Psc on the 2 days of observations. Solid lines connect consecutive observations, and broken lines show the last and first observations of a day. Data from 1987 August 11 are indicated with circles, and data from August 14 are indicated with triangles. The relative uncertainty in R is estimated to be ~5%, except for the three observations on August 14 at phases 0.08, 0.25, and 0.40, for which the uncertainty is estimated to be ~15%.

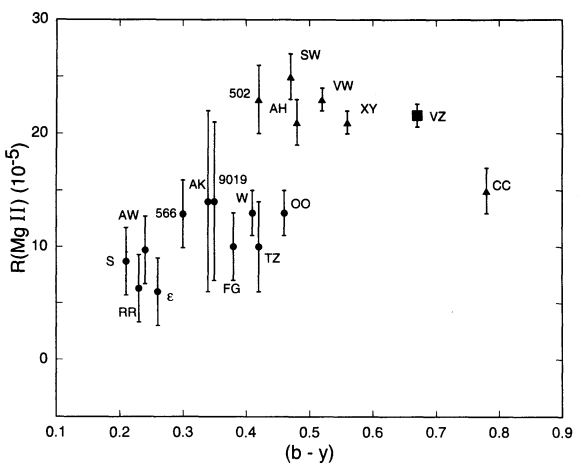

FIG. 5.—Comparison of the relative Mg II flux vs. $(b-y)$ color for W UMa–type binaries, adopted from Rucinski (1985, Fig. 4), incorporating revised values of Vilhu & Walter (1987). Triangles are for the well-determined values for large G- and K-type systems, and circles for the lower quality determinations for early G- and F-type systems. We have added VZ Psc to this figure, symbolized by a filled box. Letters and numbers beside the symbols refer to their variable star names, and are from left to right: S Ant, RR Cen, AW UMa, ϵ CrA, V566 Oph, AK Her, ADS 9019B, FG Hya, W UMa, TZ Boo, V502 Oph, OO Aql, SW Lac, AH Vir, VW Cep, XY Leo, VZ Psc, and CC Com.

VZ Psc, $(b - y) = 0.67$ (Rucinski & Kaluzny 1981). As shown in the figure, VZ Psc appears to fit in with the few other cool, short-period W UMa stars. The apparent decrease of Mg II emission with increasing color index apparent in the figure for $(b - y) \geq 0.45$ is not understood. A similar decrease in Mg II emission also occurs with decreasing orbital period (more rapid rotation). Perhaps this effect in the Mg emission is the result of a decrease in the efficiency of the magnetic dynamo for rapidly rotating stars with deep convective zones (see Rucinski 1985). A similar transition region (TR) flux ratio can be formed and yields a value for VZ Psc of log R(TR) = -4.53, in agreement with the "saturation" value of log R(TR) ≈ -4.5 found for contact binaries (Rucinski 1985).

3. GROUND-BASED SPECTROSCOPY OF VZ PISCIUM

3.1. *Observations*

Ground-based spectroscopy was obtained at the Dominion Astrophysical Observatory (DAO), using the 1.8 m telescope with Cassegrain spectrograph and intensified Reticon detector. The spectra were taken at a reciprocal dispersion of 15 Å mm^{-1} and had a resolution of 1.0 Å. A total of 40 spectra were initially obtained on two nights, 1987 August 20 and 21, approximately one week after the *IUE* spectra. All parts of the orbit were covered. The seeing was poor at the beginning of the observations on the first night, and thus we lengthened the exposure times for the first eight observations to an average of 20 minutes. Thereafter, the exposure times averaged 8 minutes, which corresponds to 0.022P. To check for consistency in the radial velocity curves, seven additional spectra were obtained at phases near quadrature on 1988 November 11, with average exposure times of 11 minutes.

The spectra were obtained for the primary purpose of monitoring the Ca II H and K emission with time and phase. The spectra covered the wavelength interval $\lambda\lambda$3920–4350, and thus they could also be used to derive absorption-line velocities of the components. Examples of unrectified spectra at phase 0.00 and 0.25 are shown in Figure 6.

The spectra were first wavelength calibrated using an Fe-Ar comparison lamp, and then the continua were rectified. This was accomplished using the program REDUCE (Hill, Fisher, & Poeckert 1982; Hill & Fisher 1986). The individual spectra were examined for spectra types, and a classification of K3–K5 was assigned with no apparent variation with phase. This is in agreement with the earlier spectral classifications of the system as K5 (Lee 1984) and K4–5 (Stephenson 1986), based upon objective prism spectra. The Balmer lines at Hγ and Hδ show clear evidence of infilling with emission, which is consistent with the emission in Hα discussed later.

3.2. *Absorption-Line Velocities*

The radial velocities of the components were determined by cross-correlating the spectra of VZ Psc with a similar spectral type, radial velocity standard star. In short-period binaries, the absorption lines are very broad and blended, and cross-correlating the spectra gives a more reliable method to determine the velocities than does line-by-line measurements. The interval of spectrum from 4000 to 4270 Å was used, which avoided the broad Ca II H and K lines and the G-band at λ4300. The spectra were converted to $1n\lambda$, and cross-correlated using the program VCROSS (Hill 1982). The radial velocity standard star used was HD 213947 (K3 V, Vr = +17.6 km s^{-1}), which was observed on the two nights in 1987 August.

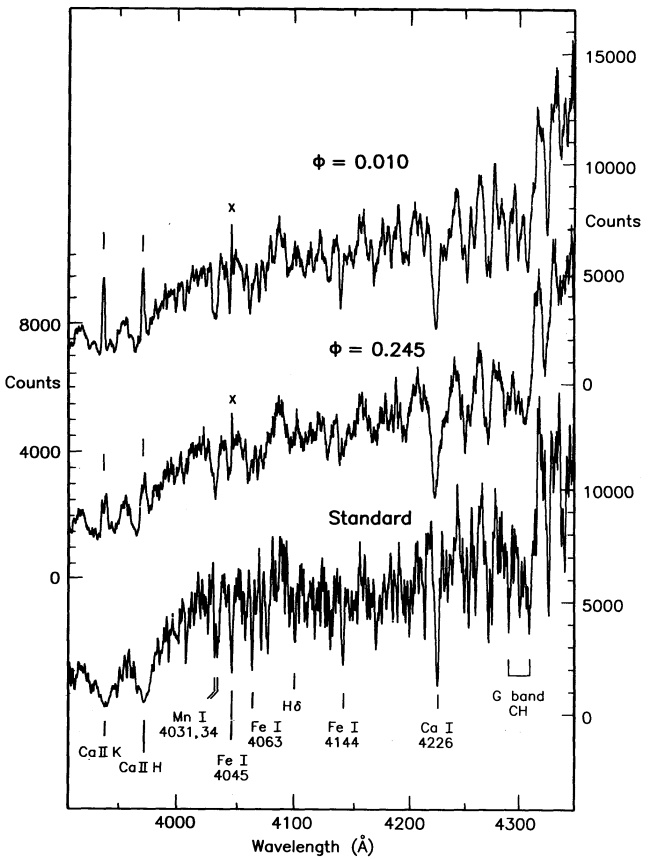

FIG. 6.—Examples of visible spectra of VZ Psc. The scale of the vertical axis is arbitrarily shifted. The spectra plotted are as follows: *top*, R72872276 (phase = 0.010); *middle*, R72872294 (phase = 0.245); *bottom*, velocity standard HD 219347 (K3 V). A number of the stronger absorption lines are labeled, and the Ca II emission features are marked. (Crosses in the VZ Psc spectra indicate terrestrial emission lines superimposed on the stellar spectra.)

We measured a radial velocity for HD 213947 of 17.4 ± 1.6 km s^{-1}, based upon the two best quality spectra we obtained. This is in good agreement with the IAU velocity of 17.6 km s^{-1}, and thus our velocities should be on the standard system.

The cross-correlation function (CCF) profiles varied from single components at conjunction to clearly resolved double components at quadrature. To measure the radial velocities, the CCF profiles were fitted simultaneously by two (or, at conjunction, one) Gaussian functions, the centers of which were taken as the component velocities. The radial velocity results are listed in Table 4, where we list the Heliocentric Julian Date (HJD) of midexposure, the phase derived from the ephemeris listed earlier (eq. [1]), and the velocities of components 1 and 2 (where component 1 is the component approaching us at phase 0.25). The spectra at phases between quadrature and conjunction were less clearly resolved, and some of their CCF profiles could not be fit reliably. The CCF profile of component 2 was slightly distorted around phase 0.75, which made the fit to both components less certain. Examples of the CCF profiles at the two quadratures are shown in Figure 7. The less certain velocity values are indicated with colons in Table 4 and were given reduced weight in the velocity-curve solution. The CCF profile of component 1 was always larger than that of component 2, with a ratio of equivalent areas of R(EA) = 0.45 within ±0.10P of the two

TABLE 4

JOURNAL OF VISIBLE-BAND SPECTROSCOPIC OBSERVATIONS OF VZ PISCIUM

A. 1987–1988 OBSERVATIONS

Image Number	HJD (2,440,000+)	Phase	V_1 (km s^{-1})	V_2 (km s^{-1})	R(EA)	$V_{1,em}$ (km s^{-1})	$V_{2,em}$ (km s^{-1})	EW_K (Å)	EW_H (Å)
R72872230.....	7027.7969	0.089		−53	...	...	...	...	...
R72872232.....	7027.8222	0.186	−133	118	0.48	...	...	...	...
R72872234.....	7027.8413	0.259	−125	152	0.22	...	...	...	...
R72872236.....	7027.8580	0.323	−124	130	0.40	−131	117	2.68	...
R72872238.....	7027.8729	0.380	−104	123	0.39	−108	75	2.24	...
R72872240.....	7027.8840	0.422	...[a]		...	+3		2.39	...
R72872242.....	7027.8944	0.462	−27		...	−7		2.41	...
R72872244.....	7027.9038	0.498	−17		...	−14		2.29	...
R72872247.....	7027.9434	0.650	80:[b]	−153	0.61:	101	−92	2.62	3.60
R72872254.....	7027.9705	0.753	84	−156	0.54:	97	−118	2.54	3.47
R72872256.....	7027.9788	0.785	88	−153	0.54:	96	−151	2.30	4.02
R72872258.....	7027.9875	0.818	84	−155	0.31	108	−116	2.37	2.96
R72872260.....	7027.9969	0.854	67	−149	0.17	77	−116	2.35	3.38
R72872263.....	7028.0076	0.895	32:[b]	...	...	80	−108	2.03	3.73
R72872274.....	7028.8108	0.970	−1		...	49	−128	...	...
R72872276.....	7028.8212	0.010	−24		...	...		...	...
R72872278.....	7028.8292	0.040	−29		...	−3		3.10	2.87
R72872280.....	7028.8365	0.068	−47		...	−14		2.99	3.12
R72872282.....	7028.8441	0.097	−67	...	...	+2		3.11	3.01
R72872284.....	7028.8521	0.128	−97	156:[b]	0.19	−7		3.25	3.29
R72872286.....	7028.8580	0.150	−107	153:[b]	0.21	+9		3.28	3.41
R72872288.....	7028.8650	0.177	−115	151:[b]	0.28	−114	84	2.89	3.41
R72872290.....	7028.8705	0.198	−128	143	0.36	−134	112	3.01	3.36
R72872292.....	7028.8768	0.222	−139	133	0.52	−162	83	3.37	2.74
R72872294.....	7028.8827	0.245	−135	141	0.36	−118	155	3.33	3.40
R72872296.....	7028.8886	0.268	−142	138	0.42	−160	115	3.16	3.26
R72872298.....	7028.8945	0.290	−135	139	0.43	−162	121	3.22	3.54
R72872300.....	7028.9007	0.314	−132	138	0.51	−138	126	3.28	2.92
R72872308.....	7028.9295	0.425	...[a]		...	−148	107	3.18	2.90
R72872310.....	7028.9372	0.454	−25		...	+20		3.07	3.13
R72872312.....	7028.9448	0.483	−14		...	+13		3.14	3.36
R72872314.....	7028.9518	0.509	−11		...	+6		3.11	2.87
R72872316.....	7028.9594	0.539	−12		...	+3		2.95	3.15
R72872318.....	7028.9663	0.565	...		...	−6		3.28	2.83
R72872320.....	7028.9729	0.590	...[a]		...	−10		3.02	2.97
R72872322.....	7028.9795	0.615	54	−146	0.37	−2		3.09	3.01
R72872324.....	7028.9868	0.643	73	−141	0.43	−9		3.08	2.69
R72872326.....	7028.9934	0.669	86	−152	0.48:	88:	−81:	3.14	3.17
R72872328.....	7029.0004	0.695	90	−152	0.51	125	−62:	2.70	2.91
R72872330.....	7029.0077	0.723	82	−163	0.36:	114	−108	...	...
R72885886.....	7445.7267	0.765	122	−132	0.71	...	...	...	...
R72885888.....	7445.7343	0.794	118	−134	0.64	...	...	...	...
R72885889.....	7445.7413	0.821	92	−163	0.42	...	...	...	...
R72885891.....	7445.7489	0.850	96	−150	0.38	...	...	...	...
R72885909.....	7445.8465	0.224	−151	117	0.70	...	...	...	...
R72885911.....	7445.8572	0.264	−145	129	0.65	...	...	...	...
R72885913.....	7445.8659	0.298	−135	129	0.60	...	...	...	...

B. 1983–1984 OBSERVATIONS

Image Number	HJD (2,440,000+)	Phase	V_1 (km s^{-1})	V_2 (km s^{-1})	R(EA)
P92332.....	5572.9709	0.569	2		...
P92333.....	5572.9813	0.609	−10		...
P92411.....	5592.8557	0.681	119	−131[b]	1.46
P92412.....	5592.8626	0.707	100	−177:[c]	0.64
P92413.....	5592.8685	0.730	105	−151[b]	...
P92414.....	5592.8772	0.763	115	−140[b]	...
P92415.....	5592.8828	0.784	118	−124[b]	0.88
P92416.....	5592.8880	0.804	104	−131:[c]	0.62
P92417.....	5592.8946	0.830	110	−127[b]	...
P92418.....	5592.9033	0.863	98	−120[b]	1.05
P93181.....	5898.9387	0.250	−128	121	0.44
P93182.....	5898.9498	0.292	−125	125	0.50
P93183.....	5898.9564	0.318	−113	132	0.40
P93184.....	5898.9612	0.336	−90	141	0.21
P93269.....	5904.9357	0.204	−127	141	0.53
P93270.....	5904.9419	0.228	−136	126	0.55
P93271.....	5904.9485	0.253	−142	115	0.61

[a] Two components, but too blended to measure as separate.
[b] Weight = 0.5.
[c] Weight = 0.0.

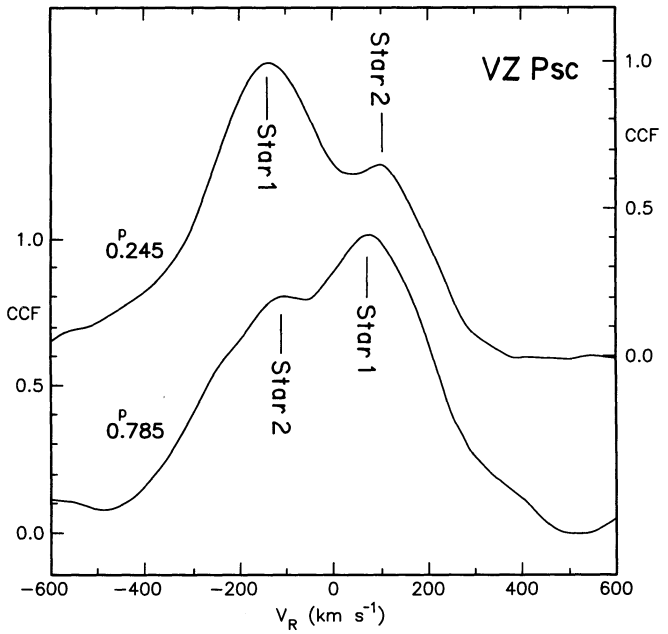

FIG. 7.—Examples of the cross-correlation function profiles of VZ Psc at the two quadratures. The upper profile is of spectrum R72872294 (phase = 0.245) and the lower profile is of R72872256 (phase = 0.785).

quadratures. Note that taken alone, the seven spectra from 1988 indicate a higher ratio of 0.59. The values of this ratio R(EA) are listed in column (6) of Table 4.

The radial velocity curves based upon these velocities are ploted in Figure 8*a*. It can be seen that the velocities corresponding to phases where only a single peak was measured seem to follow the velocity curve for component 1. The radial velocities were analyzed using a spectroscopic binary program of G. Hill. The two radial velocity curves were first solved separately and yielded solutions with systemic velocities which differed by 8 km s^{-1}. This is a rather large amount but is not entirely surprising, since the data points have a large scatter among themselves, as is seen in Figure 8*a*. We then solved both velocity curves simultaneously. This yielded a spectroscopic mass ratio of 0.76 ± 0.04, based upon 30 double-lined spectra plus two spectra in which only component 1, the more massive star, could be measured accurately. This value is significantly different than the value of 0.92 ± 0.03 obtained by Hrivnak & Milone (1989, hereafter HM89), based upon half as many photographic spectra. An examination of the CCF profiles of both these new spectra and the older spectra of HM89 shows that the two components are not nearly as well resolved for VZ Pcs as for the other short-period binaries we have studied (Hrivnak 1988, 1989, 1993). Also, as we have mentioned, a noticeable distortion is present in the spectra around phase 0.75. Rather than attempting to judge between these new data and earlier photographic data of HM89 or suggesting that the mass ratio has changed, we decided to incorporate the older spectra of HM89 into a new combined study. Consequently, we cross-correlated the 1983 and 1984 spectra of HM89 with our present radial velocity standard, and have listed these velocities in the lower portion of Table 4. Taken alone, the 1983–1984 spectra yield a mass ratio of $q = 0.90 \pm 0.03$, not significantly different from the value derived by HM89 in their analysis using a different standard star. These data are plotted in Figure 8*b*, using a different symbol, along with our new data. Although one can see the suggestion of a slight systematic difference between the two data sets, in fact this appears to be no greater than that seen between the new 1988 data and the 1987 data. This may indicate some real variation in the velocity curves caused by complications in the system or complications in the spectra. In an attempt to get the most reliable radial velocity solution for the system, we decided to solve the velocity curves using all the data. The results for this and the previously discussed solutions are given in Table 5. This combined solution results in a mass ratio of 0.80 ± 0.03. The semi-amplitudes of the two velocity curves lie between the values based upon the separate analyses of the 1987–1988 data and the 1983–1984 data of HM89. The fit of the velocity solution to all observed data is shown in Figure 8*b*. We believe that this new radial velocity solution is superior to that of HM89, primarily because it is based upon more data. This system has been harder to solve than most short-period binaries studied as

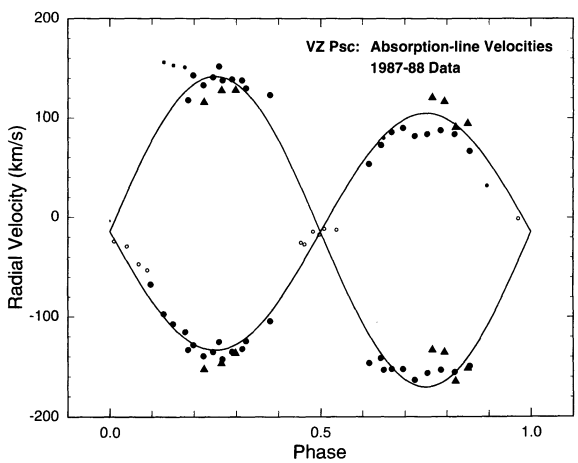

FIG. 8*a*

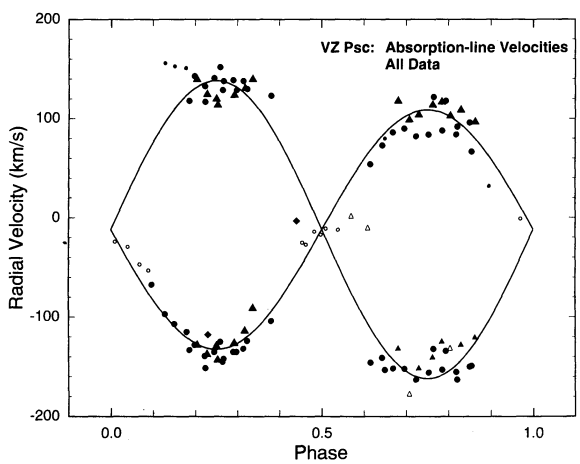

FIG. 8*b*

FIG. 8.—(*a*) Radial velocity curves of VZ Psc. Data are plotted with different symbols, circles for 1987 and triangles for 1988. The size of the symbol is related to the weight of the velocity value in the radial velocity solution, as described in the text. The solid line represents the radial velocity solution to the 1987–1988 observations. (*b*) Combined radial velocity curves of VZ Psc, including older data. Symbols are as follows: *circle*, 1987–1988; *triangle*, 1983–1984 (Hrivnak & Milone 1989); *diamond*, 1981–1982 (Fouts 1987), Solid line represents the radial velocity solution based upon the combined 1982–1983 and 1987–1988 observations.

TABLE 5

RADIAL VELOCITY SOLUTION OF VZ PISCIUM

Element	1987–1988	1983–1984	Combined (Point-mass)	Combined (Light-curve model, without spots)
V_0 (km s^{-1}).....	-14.4 ± 4.3	-4.8 ± 3.6	-11.8 ± 2.9	-12.2 ± 1.6
K_1 (km s^{-1}).....	118.8 ± 4.4	123.8 ± 3.1	120.6 ± 2.8	125.0 ± 2.2
K_2 (km s^{-1}).....	156.7 ± 5.1	137.9 ± 4.1	150.2 ± 3.4	156.2 ± 2.5
σ_1 (km s^{-1}).....	11.4	10.9	12.8	12.4
σ_2 (km s^{-1}).....	20.1	13.6	19.8	16.1
$a_1 \sin i$ ($R_\odot$).....	0.613 ± 0.022	0.639 ± 0.016	0.622 ± 0.014	0.645 ± 0.011
$a_2 \sin i$ ($R_\odot$).....	0.809 ± 0.026	0.712 ± 0.021	0.775 ± 0.017	0.806 ± 0.013
$M_1 \sin^3 i$ ($M_\odot$).....	0.322 ± 0.019	0.256 ± 0.013	0.299 ± 0.012	0.334 ± 0.013
$M_2 \sin^3 i$ ($M_\odot$).....	0.244 ± 0.015	0.230 ± 0.011	0.240 ± 0.010	0.267 ± 0.011
q ($=M_2/M_1$)	0.758 ± 0.037	0.898 ± 0.035	0.803 ± 0.026	0.800 ± 0.018

a result of the smaller velocity separation between the components caused by a lower orbital inclination. The solution may also be complicated by the presence of large and variable starspots on the stars. This is discussed later in § 4.3.

Note that Fouts (1987) obtained two spectra of VZ Psc with the 2.5 m telescope and Shectman Reticon detector at Mount Wilson Observatory in 1981 and 1982. He measured a single radial velocity component in each of these using the cross-correlation method. His velocities fit well with those of this study and have been added for comparison to Figure 8*b*.

Although the new radial velocity study has determined a lower mass ratio for VZ Psc than that determined by HM89, it still ranks as one of the highest among the contact and near-contact binaries. The other systems with large, spectroscopically determined mass ratios are OO Aql $q = 0.83$ (Hrivnak 1989), and SW Lac, $q = 0.80$ (Zhai & Lu 1989). Typical values for contact binaries are 0.4 to 0.5 (Mochnacki 1981).

3.3. Ca II *H and K Emission*

Strong Ca II H and K emission is present on these spectra, as is seen in Figure 6. At the conjunctions, single strong emission features are seen in the cores of the H and K lines, and near quadrature the features are split into two main components. From these new spectra we measured equivalent widths and radial velocities of the emission features. To measure the equivalent widths (EWs), a rotationally broadened absorption profile was fitted to the absorption line below the apparent continuum, and then single or double Gaussians were fitted to the emission features. Radial velocities were measured from the center of these Gaussians. This provided a consistent and objective method to measure the radial velocities of the components and also the emission strengths. The emission components were more clearly resolved into two components in the K line than in the H line, which was often a rather broad feature. Due to an oversight, the Ca II emission was not measured for the seven 1988 spectra, although it was present in them.

The radial velocities measured for the H and the K components in each spectrum were usually in good agreement, although the H line was less well resolved and was assigned lower weight, and weighted average values are listed in Table 4. These Ca II emission velocities were plotted versus phase in Figure 9. For comparison, we have also plotted the radial velocity curves derived from the combined solution to the absorption-line velocities. It can be seen that the emission components generally follow the centers of the two components, except around the conjunctions, where the single components have values near the systemic velocity. This indicates that the emission comes in general from broad regions distributed uniformly around both stars. This had been suggested in the earlier data of HM89. This result is in contrast to the K spectral type contact systems CC Com and V523 Cas, in which the emission is associated with the more massive star (Rucinski, Whelan, & Worden 1977; Milone, Hrivnak, & Fisher 1985). The difference in VZ Psc is presumably a result of the relatively larger mass of the secondary as indicated by the higher mass ratio; in CC Com, the mass ratio is 0.50 (Rucinski et al. 1977), and in V523 Cas it is 0.40 (Milone et al. 1985). There does appear to be a systematic effect in the sense that the emission velocities from component 2 indicate a smaller amplitude than do the absorption-line velocities, suggesting the emission to be centered preferentially closer to component 1 than is the center of mass of component 2. Component 1 shows the opposite effect, with the emission velocities displaying a slightly larger amplitude, suggesting the emission to be centered slightly farther away from the other star than is the center of mass of component 1.

Equivalent widths were measured for the H and K lines from the Gaussian fits. While it is hard to determine the true continua in the late-type stars, one could nevertheless search for phase-related or nightly variability in the strength of the emis-

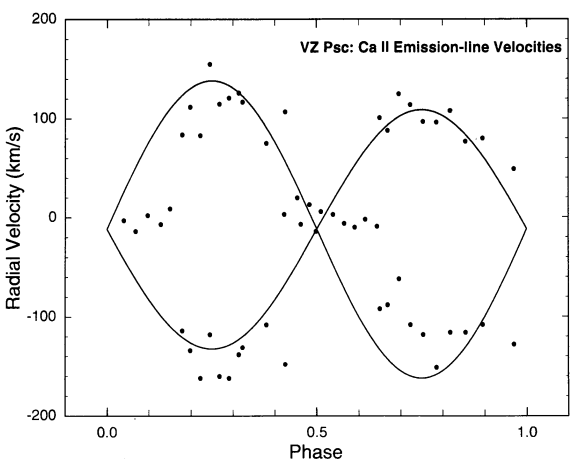

FIG. 9.—Radial velocity plot of Ca II emission features from the 1987 spectra. Solid line represents the combined solution to the absorption-line velocities.

sion features. Pseudocontinua could be determined consistently in the interval from 3910 to 3950 Å for the K line and from 3950 to 3980 Å for the H line. The total equivalent widths for the one or two emission components in the K and H lines are also listed in Table 4 in the rightmost columns. We have not included Ca II emission measurements from the first three observations of 1987 or the next five H measurements; these had longer exposure times and were more severely contaminated by moonlight.

A plot of the total equivalent width of the K line versus phase shows a clear variation between the two nights, as seen in Figure 10. The average value of the EW(K) for 1987 August 20 is 2.37 ± 0.08 Å, and for August 21 it is 3.12 ± 0.03 Å. This change could be the result of a change in the emission strength of one or both components. To investigate this further, we have calculated the nightly strengths of the individual components near quadrature, where we could clearly resolve these. It appears that the strength of the emission from component 1 has changed little, if any, while the level of emission for component 2 increased significantly from the first to the second night. Average values of the EW of the K line for component 1 were 1.08 Å and 1.27 Å and for component 2 were 1.42 Å and 1.91 Å on the nights of 1987 August 20 and 21, respectively. Thus, it seems that one can ascribe the variability on these two nights to a large change in the activity level of component 2. Note that it is component 2, the less massive star, which possesses the stronger emission features. No phase-dependent variability is apparent on these two nights.

The structure of the H line was more complicated, often appearing as a broad plateau, and we were not able to measure the EW(H) of each component to investigate this effect in the strength of the individual components. The total strength of the H line seems to vary from a lower to a higher level during the course of the first night, and it is constant at a median level during the second night.

3.4. Hα *Emission*

Another indicator of chromospheric activity in a late-type star is Hα emission. A spectrum of VZ Psc in the region of Hα was obtained by B. Bopp on 1985 October 3 and kindly made available to us. The spectrum was obtained with the KPNO Coudé Feed telescope and TI CCD, with a resolution of ~0.25 Å. The integration time was 2000 s, and it was centered at phase 0.30. The spectrum, with slight smoothing, is shown in Figure 11. We have also included for general comparison the spectrum of a rapidly rotating GO III star (HR 339, $v \sin i \sim 75$ km s^{-1}) and a K5 V star (61 Cyg A). Note that the vertical scales are different in each spectrum. The two absorption features at λ6570 are caused by strong telluric features.

Broad Hα emission is clearly seen rising about 15% above the continuum in VZ Psc. This feature is 10 Å wide, which is significantly greater than the velocity separation between components. The equivalent width in emission above continuum is approximately 1.1 Å; of course, the total emission strength is actually significantly larger, since we have not corrected for the underlying absorption. Such relatively strong emission is quite unusual among this type of short-period binary. While Hα emission has been detected spectroscopically in several W UMa and short-period RS CVn binaries, it has usually appeared in these other cases as infilling of absorption lines, which simply reduced their depths, but not an emission above the continuum (Barden 1985). We are not aware of any W UMa binary in which Hα emission has been seen above the continuum level. In the short-period RS CVn binary HD 8358 (G5; $P = 0^d.516$), Hα is seen in emission at a level of 10% above continuum (Bopp et al. 1985).

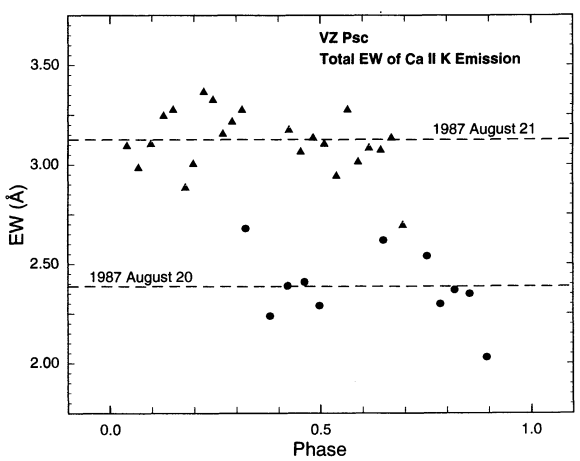

FIG. 10.—Variation of equivalent width (EW) of Ca II K line with orbital phase and with time. The data from 1987 August 20 (*circle*) and August 21 (*triangle*) are distinguished with different symbols, and dashed lines indicate the average values for each night.

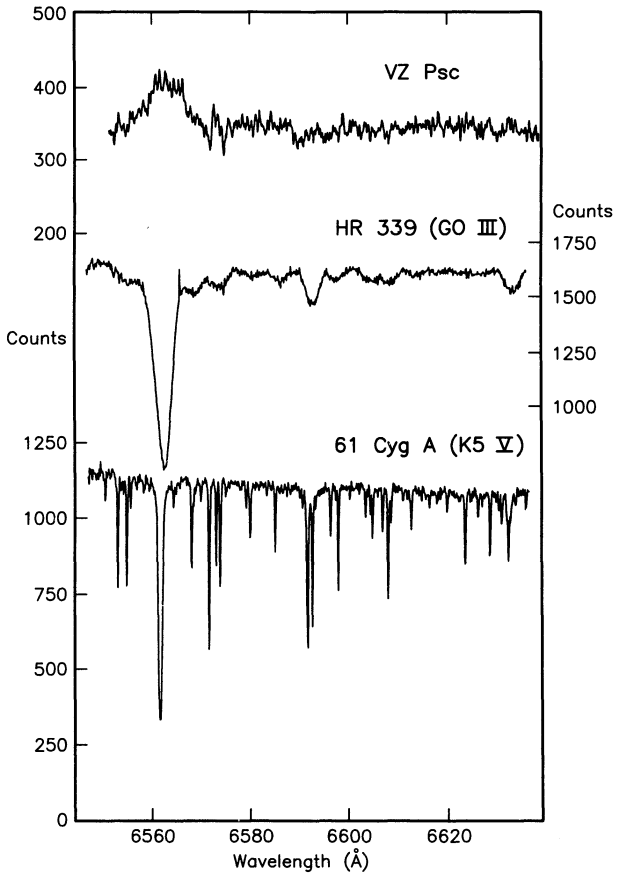

FIG. 11.—Spectrum of VZ Psc in the region of Hα, showing emission. Two additional stars are shown for comparison, the rapidly rotating G0 III star HR 339 and the dwarf K5 star 61 Cyg A.

4. LIGHT-CURVE STUDIES OF VZ PISCIUM

4.1. *Previous Studies*

As already discussed in § 1, the light curves of VZ Psc display shallow minima of unequal depths and at times asymmetries in the shapes and heights of the maxima (see Bradstreet 1985; Samec 1989). Most of the light variation is caused by the oblate shape of the stars (ellipsoidal effect); very little is caused by the eclipses of the stars. Early solutions of the photoelectric light curves by Bradstreet (1985), Hrivnak & Milone (1989), and Barone et al. (1989) indicate a greatly overcontact configuration for VZ Psc and a very large temperature difference between components of $\Delta T \sim 800$–1200 K. The large temperature difference between the stars and the large fill-out factor of up to 90% lead to the implausible situation that VZ Psc is in a state of extreme overcontact physically, yet is far from a state of thermal equilibrium. As pointed out by Samec (1989), this is a physically unrealistic situation, and the binary would be in definite violation of the thermal-relaxation–oscillation (TRO) theory proposed by Lucy (1976) and Flannery (1976). In the TRO theory, systems which have poor thermal contact (components with large temperature differences) should be semidetached binaries, or in a state of marginal or shallow contact. The reevaluation of the light curves by Maceroni et al. (1990) with a light-curve synthesis program incorporating starspots appears to have solved most of the problems with VZ Psc. In their model, two cool, dark spots covering about 6% of the surface of the cooler star are located on its outer hemisphere. This spotted hemisphere is visible primarily during the phase interval 0.9–0.1, causing the minimum at phase 0.00 to be significantly deeper than that at phase 0.50. Thus, the difference in the minima is explained by cool, dark spots and not by a large temperature difference between components. These two spots also make the primary minimum wider, which also fits the observation that the maxima are shifted from phases 0.25 and 0.75 to phases closer to the second minimum.

4.2. *New Light-Curve Solutions*

We decided to do a new solution of the light curves, since (a) we have an improved value of the mass ratio, (b) new multicolor light curves have been published, and (c) we also wanted to investigate a model with a hot spot visible at phase 0.50. The fit to the B and V light curves simultaneously should yield a more constrained solution than that of the single red light curve previously analyzed. The B and V light curves of Samec (1989) were used in the following analysis. They were gathered into normal points within phase intervals of $0.01P$ and normalized to the mean of the two maxima.

We used the synthetic light curve and differential corrections programs of Wilson & Devinney (Wilson & Devinney 1971; Wilson 1979), which have been recently modified to incorporate spots and to adjust their properties by differential corrections (Wilson 1992). Parameter values were fixed for the temperature of the more massive star: component 1 (T_1), the gravity darkening exponent (g), the bolometric albedo (A), and the mass ratio (q). Values for the limb darkening (x_V, x_B) were taken from the tables of Al-Naimiy (1978), and third light (l_3) was fixed at 0.00. Note that we recently obtained a CCD image of the field of VZ Psc at Kitt Peak National Observatory and found no close visible companion which could contribute third light to the system. The parameters which were permitted to adjust were the orbital inclination (i), the temperature of the less massive star (T_2), the wavelength-dependent luminosity of component 1 ($L_{1,\lambda}$), and the values of the modified equipotential surface of each component (Ω_1, Ω_2). Initial values of these were set such that the inclination corresponded to main-sequence masses for the two components, the equipotentials corresponded to main-sequence radii, and the two components had the same temperatures.

We explored four basic models which incorporated cool or hot spots on components 1 or 2. For each spot, one could in principle adjust its longitude (l), co-latitude (b), radius (r), and temperature factor (TF, local spot temperature relative to local temperature in absence of spot). We found the radius and temperature factor of each spot to be highly correlated, such that one could increase the effect of a cool spot by either increasing the radius or decreasing the temperature factor. The very shallow eclipses in this system prevent one from determining these two parameters separately. Thus, we decided to keep the temperature factors fixed and allow the spot radii to vary. The spots were arbitrarily constrained to lie at the equator, to reduce the numer of free parameters. It was found that models with two spots give a significantly better fit to the depth and width of the affected minimum than did one spot, so we proceeded to fit the light curves with two spots.

We began by exploring models with two cool spots on the outer hemisphere of component 2 (less massive star, in front at phase 0.00), which contribute to make the minimum at phase 0.00 much deeper. This is the model advanced by Maceroni et al. (1990). The inclination was adjusted slightly from the initial value to give a reasonable fit to the secondary minimum, which we initially assumed to be unspotted. Following the example of Maceroni et al., we began with a detached configuration. The two-spot model was initiated with spots of radius $r = 30°$, temperature factor $TF = 0.80$, and situated at longitudes symmetric about the back point of component 2 ($l = 180°$) at $l_1 = 150°$ and $l_2 = 210°$. These parameters produced a reasonably good fit to the primary minimum, and we fixed TF at this value. The binary parameters (i, T_2, Ω_1, Ω_2, $L_{1,\lambda}$) and spot parameters (l_1, r_1, l_2, r_2) were permitted to adjust together in the differential corrections program. Several iterations with the differential corrections program were made, until the parameters all converged such that the indicated adjustment to the parameters were all less than or on the order of the errors in the parameters. In some cases, this led to a very high correlation among the parameters, and in these cases the method of multiple subsets (MMS) was used, in which the spot parameters were adjusted together with T_2 and Ω (usually) or together with i and L_1 (only occasionally, since this subset usually had high correlations). The initially detached configuration converged to an overcontact configuration, with a fill-out factor of $FF = 33\% \pm 16\%$ and a value of T_2 more than 200 K higher than T_1. The fit of the model to the observed light curve was reasonably good, although there remained regions of the light curve, in particular around primary minimum, in which the model deviated systematically from the observations. The parameters for this solution are listed as model 1 in Table 6, along with their standard errors. Owing to parameter correlations, the uncertainties in the parameters are rather large. (Note that the errors listed are those obtained for a simultaneous solution of the binary and spot parameters, which takes into account correlations between the various parameters; however, these do not account for any uncertainty in the mass ratio, which was held fixed.) The weighted sum of the residuals squared is also listed, for comparison of the good-

TABLE 6

LIGHT-CURVE SOLUTIONS OF VZ PISCIUM

A. PARAMETERS HELD FIXED

Parameter	Value
T_1 (K)	4500
$A_1 = A_2$	0.50
$g_1 = g_2$	0.32
$x_{1,V} = x_{2,V}$	0.83
$x_{1,B} = x_{2,B}$	0.99
l_3	0.00
$q\ (=M_2/M_1)$	0.80
$\Omega_{\rm inner}$	3.417

B. PARAMETERS VARIED

Parameter	Model 1 (Cool spots on 2; mode = 3; configuration = overcontact)	Model 2 (Cool spots on 1; mode = 3; configuration = overcontact)	Model 3 (Hot spots on 1; mode = 3; configuration = marginal overcontact)	Model 4 (Hot spots on 2; mode = 4; configuration = marginal undercontact)
i	47° (3)	47° (3)	49° (1)	48° (1)
T_2 (K)	4740 (120)	4700 (320)	3890 (130)	4110 (060)
Ω_1	3.27 (7)	3.28 (10)	3.41 (1)	3.417[a]
Ω_2	3.27[b]	3.28[b]	3.41[b]	3.44 (4)
FF (% overcontact)	33 (16)	30 (22)	2 (2)	−5 (9)
$L_{1,V}/(L_{1,V} + L_{2,V})$	0.48 (2)	0.49 (5)	0.754 (10)	0.685 (05)
$L_{1,B}/(L_{1,B} + L_{2,B})$	0.46 (3)	0.47 (6)	0.794 (09)	0.714 (06)
Spot Parameters				
l_1	127° (4)	297° (21)	122° (1)	299° (2)
r_1	36° (4)	28° (10)	19° (1)	32° (2)
TF_1	0.80[a]	0.80[a]	1.20[a]	1.20[a]
l_2	222° (10)	15° (16)	233° (2)	57° (2)
r_2	36° (2)	41° (11)	18° (1)	29° (2)
TF_2	0.80[a]	0.80[a]	1.20[a]	1.20[a]
ΣwR^2	0.0044	0.0045	0.0038	0.0036
Bradstreet's Red Light Curve				
$x_{1,r} = x_{2,r}$	0.76[a]	0.76[a]	0.76[a]	0.76[a]
$L_{1,r}/(L_{1,r} + L_{2,r})$	0.486 (1)	0.496 (1)	0.727 (1)	0.667 (1)
l_1	115° (1)	298° (2)	140° (2)	315° (2)
r_1	37°.9 (8)	34°.9 (7)	15°.8 (3)	24°.3 (5)
TF_1	0.80[a]	0.80[a]	1.20[a]	1.20[a]
l_2	240° (1)	58° (2)	235° (2)	61° (2)
r_2	40°.5 (7)	37°.1 (6)	15°.9 (3)	25°.6 (4)
TF_2	0.80[a]	0.80[a]	1.20[a]	1.20[a]
ΣwR^2	0.0025	0.0034	0.0021	0.0019

NOTE.—Standard errors in the last digit are given in parentheses (not probable errors, as are usually listed in Wilson-Devinney analyses).

[a] Parameters held fixed.

[b] $\Omega \equiv \Omega_2$.

ness of this fit with others discussed later. We also examined the fit of this solution to the observed red light curve of Bradstreet (1985). A good fit could be obtained with the binary parameters kept fixed at the values determined from the solution to the B and V light curves, and allowing an adjustment to the longitudes and radii of the two spots. These results are also listed in Table 6.

The second model we investigated was that with the two cool spots on the inner hemisphere of component 1. This would also produce a deeper minimum at phase 0.00. We were not able to get a stable convergence of the parameters, even using the MMS. With trial and error, we did arrive at a reasonable fit, which was the best we could do. The uncertainties in the parameters are quite large. This was also an overcontact configuration, with a fill-out factor of 30% ± 22% and a value of T_2 which was 200 K higher than T_1. The fit to the B and V light curves is comparable to that of model 1. We also fitted the red light curve of Bradstreet, although this was not as good as in the case of the cool spots on star 2 (model 1). The parameters determined from this model are listed as model 2 in Table 6.

We next investigated the models with hot spots visible at phase 0.50, which would reduce the depth of the light curve at this phase. We began with two hot spots on the outer hemisphere of component 1 (more massive star, in front at phase 0.50). The initial binary parameters were derived from a fit to what we assumed to be the unspotted portion of the light curves, that around the primary minimum. We fixed the temperature factor at $TF = 1.20$. We began analyses with both detached and overcontact initial configurations. In both cases, the solutions converged to a marginally overcontact configuration. The fill-out factor was 2% ± 2%, and thus the configuration is only slightly overcontact and not significantly different from marginal contact. T_2 is lower than T_1 by more than 600 K. The parameters for this solution are listed as

model 3 in Table 6. The fits to the entire B and V light curves are very good and are even better than the fits produced by the models with cool spots. We then fitted the Bradstreet red light curve, using the same binary parameters but allowing the spot parameters to vary, and a very good fit was obtained, again better than that for the models with cool spots. These results are also listed in Table 6.

Lastly, we investigated a solution with the hot spots again visible at phase 0.50, but this time on the inner hemisphere of component 2 (less massive star, behind at phase 0.50). Starting with both detached and overcontact initial configurations, the solution converged to a configuration which was semi-detached, with star 1 filling its Roche lobe and star 2 slightly smaller than its Roche lobe, possessing a value of Ω which would lead to a fill-out factor of $-5\% \pm 9\%$. Within this large uncertainty, the configuration can be regarded as slightly under marginal contact or in marginal contact. T_2 is lower than T_1 by about 400 K. This solution produced the best fits to the B and V light curves, similar to and slightly better than those of model 3. This is quantified by the smallest weighted sum of the residuals squared, which is also listed for each solution in Table 6. We again fitted the Bradstreet red light curve, with only the spot parameters permitted to vary, and again this configuration gave the best light-curve fit. The fits of this model to the B and V light curves are shown in Figure 12, and the fit to the red light curve is shown in Figure 13.

Thus, we find that we can get good fits to the light curves of VZ Psc with either hot or cool spots, but with the hot spot models producing significantly better fits to the observed light curves. We regard these as representative solutions of the light curves, but not unique ones because of the low inclination and complication of spots. Maceroni et al. (1990) made a similar claim with respect to their solution with two cool spots. We compare briefly our cool spot model (model 1) with the similar one of Maceroni et al., who used a different mass ratio ($q = 0.92$) and were fitting only the red light curve. They obtained a slightly semidetached solution with component 1 slightly inside its Roche lobe. Their spots were smaller ($r = 21°$) than the two in our solution. This is due in part to their allowing the spots to be located at a latitude above the equator. We find that by confining the spots to the equator, the radii of the two cool spots must be larger than 25° to fit the width and depth of the primary minimum, and that an overcontact solution provides a significantly better fit to the B and V light curves. Remember that we arbitrarily selected equatorial spots, since the eclipses are far too shallow to allow eclipse maps to determine unambiguously the spot latitudes. By confining the spots to the equator, we simply reduce the number of free parameters in the solution. We do note, however, that in most chromospherically active stars the spots seem to be located at midlatitudes or near the poles (see, e.g., the recent review by Guinan & Giménez 1993). Moving the spots to midlatitudes would require smaller spots, since they would then be nearly perpendicular to our line of sight (since we are assuming implicitly that the rotation axes of the stars are perpendicular to the orbital plane, which has an inclination of about 50° to the plane of the sky).

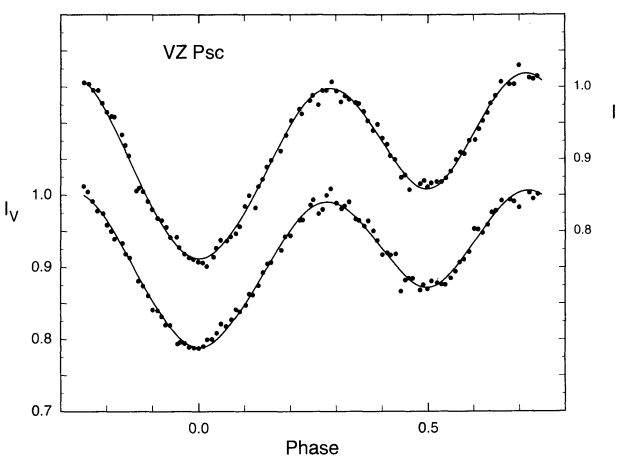

FIG. 12.—The fit of light-curve model 4 (hot spots on component 2) to the normal-point B and V light curves of Samec (1989).

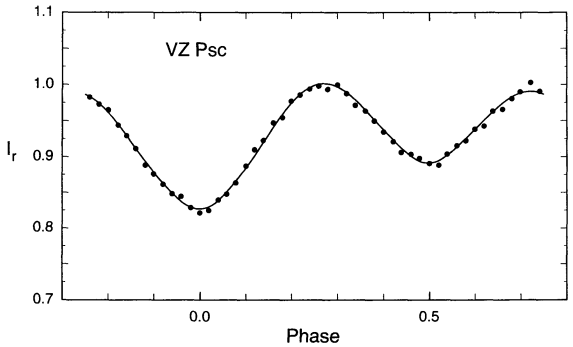

FIG. 13.—The fit of light-curve model 4 (hot spot on component 2) to the normal-point red light curve of Bradstreet (1985).

Some additional information to help decide which one of the models is the most likely can be found in the history of the light-curve variation, from the Ca II emission, and from the absorption-line strengths. A study of the light-curve variation, which we discuss in the next subsection (4.3), indicates that the largest changes in the light curve occur in the secondary minimum. This favors a model with active regions (spots) visible around phase 0.50, such as are found in the hot spot models, models 3 and 4. If the hot spots are associated with enhanced Ca II emission, as seems likely, then this might show up in the Ca II study. The Ca II radial velocity curves suggest enhanced emission on the inner hemisphere of component 2, which is consistent with model 4. However, there is also an indication of enhanced emission on the outer hemisphere of component 1, consistent with model 3. The Ca II emission is stronger for component 2, again favoring model 4. In § 3.1, we noted that the CCF profile of component 1 was always larger than that of component 2, with a ratio of equivalent areas of $R(\mathrm{EA}) = 0.45$ near the two quadratures. This would suggest a relative light fraction of 69% for component 1 and 31% for component 2 in the blue part of the spectrum, which is identical with the values found in the model with hot spots on component 2 (model 4) and clearly inconsistent with the cool spot models. Based upon the light-curve modeling and this additional information, it can be seen that the array of observations clearly supports the hot spot models, with the most likely model of the system the one with hot spots on the inner hemisphere of component 2 (model 4). In Figure 14 we display a three-dimensional representation of this configuration (model 4) at the time of Samec's observations, using the program Binary Maker (Bradstreet 1993).

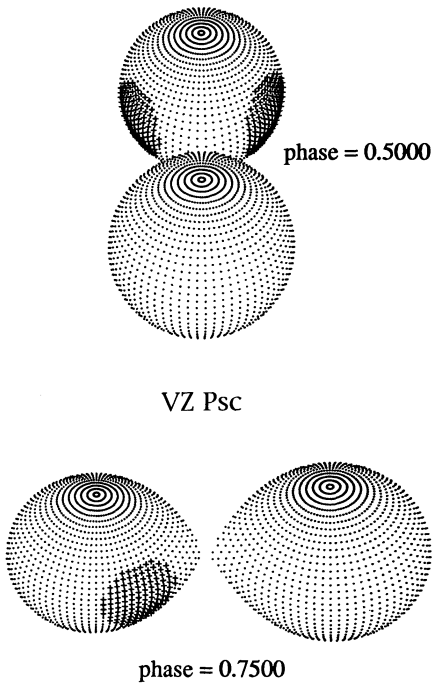

FIG. 14.—Three-dimensional representations of VZ Psc in the overcontact configuration, with two hot spots on component 2.

4.3. *Effect of the Light Distribution on the Radial Velocity Solution*

We note that the light distribution on the components of a binary star system can, in principle, affect the observed radial velocities by shifting the projected light centers away from the projected mass centers. (It is the velocity of the two light centers which we measure in the absorption-line spectra). The radial velocity curves presented in § 3.2 were solved assuming that the stars were point masses, with no consideration of the light distribution on the components or interaction effects between the components. We decided to investigate this effect by using the Wilson-Devinney program to solve for the velocity-curve parameters based upon the light distribution determined for the binary (Wilson 1979). We first investigated the effect of the light distribution on the distorted stars, initially neglecting the effect of the two hot spots on component 2. This resulted in an $\sim 4\%$ increase in K_1 and K_2, and no change in the mass ratio $q = 0.80 \pm 0.02$. This change in the semiamplitude occurs because the projected light centers of the the two components are slightly closer together than are the projected mass centers. We next investigated the effect on the velocity-curve parameters of including the full light-curve model, including the two hot spots on component 2 (model 4). This resulted in a 3% increase in K_1 and an 11% increase in K_2, as compared to the combined point-mass model listed in Table 5, and a change in the mass ratio to $q = 0.75 \pm 0.02$. This result for K_2 is easily understood, since the increase in light caused by the spots on the inner hemisphere of component 2 moved the light center of component 2 even farther away from the center of mass and closer to component 1. At this point, one can see that the velocity parameters depend on the light-curve model in a significant way, and in particular upon the presence and location of the hot spots in the model. These are factors which appear to vary with time, as indicated by the change in position of the spots in the solutions of the light curves of Samec from 1986 and Bradstreet from 1982 and as discussed further in the next section. The parameters of the hot spots we determined from the fit to the 1982 red light curve of Bradstreet are different from those found by fitting the 1986 *B* and *V* light curves of Samec. In particular, the spots are about 20% smaller in radius, and spot 1 is located 15° closer to the substellar point in the model to fit the Bradstreet light curve than in the model to fit the Samec light curves (Table 6). This change in spot parameters in the solution to the Bradstreet light curve changes the effect of the spots on the velocity semiamplitude of component 2 by reducing it by $\sim 2\%$ at first quadrature and causing it to vary between an $\sim 5\%$ increase in the phase interval 0.60–0.70 and an $\sim 6\%$ decrease in the phase interval 0.80–0.90. These are significant changes. Thus, one can see that to really model the varying light curves and velocity curve of VZ Psc consistently, one needs to have observations made simultaneously in time or nearly so. It may indeed be that the differences seen in the velocity observations from different years are the result of changes in the light distribution caused by changes in the spots among the different years. Since none of the light and velocity curves have been observed in the same season, we are not in a position to do such a consistent analysis. Thus, we will continue to use for our velocity-curve analysis the combined velocity data from the different years. We still face the question of whether we should revise the mass ratio used in our light-curve model. We did investigate the effects on the light-curve parameters of adjusting model 4 (two hot spots on component 2) with a mass ratio of 0.75, which was the value determined for the solution of the velocity curves based on the light-curve model with hot spots. It converged to a similar marginally semidetached solution, with none of the other parameters (except Ω and q) significantly different from the values shown in Table 6 for model 4.

These results are, of course, highly model dependent, and while the evidence favors the model with two hot spots on component 2, we are hesitant to revise the mass ratio to the value of 0.75 determined from this spot model solution to the radial velocity curves. Thus, we have chosen not to include the effects of the hot spots in our velocity-curve solution. However, the marginal contact configuration seems to be well established, since it is found in both our hot spot models (models 3 and 4). This marginal contact configuration, without the inclusion of hot spots, results in a light distribution that has the effect of leading to an underestimation of the values of the semiamplitudes of the velocity curves by about 4%. We have listed this solution to the velocity curves, based upon the light-curve model without spots, in Table 5 along with our point-mass solutions, and we will used it in the determination of the absolute parameters of the system.

4.4. *Light-Curve Variability*

The light curves of VZ Psc vary with time. This was first reported by Bradstreet (1985) and subsequently discussed by Samec (1989) and Hrivnak & Milone (1989). However, no previous systematic study of the light-curve variability has been published.

Photoelectric light curves of VZ Psc (or in some cases only partial light curves) have been published by Eggen (1967), Bradstreet (1985), Poretti (1984), Davidge & Milone (1984), and Samec (1989). Because different comparison stars were used in these studies, only relative measures of the light-curve properties could be obtained. To compare the various light curves, we determined the depth of each of the two minima

TABLE 7

VARIATIONS IN THE LIGHT CURVES OF VZ PISCIUM

Epoch	Filter	Depth min I	Depth min II	Difference min I − II	Difference max I − II	Reference[a]
1967.51.....	V	+0.249 (18)	+0.219 (18)	+0.030 (18)	+0.010 (10)	1
1980.87.....	None (λ_{eff} = 5500)	+0.228 (15)	+0.174 (15)	+0.054 (15)	~0.00 (15)	2
1981.59.....	*V*	+0.238 (12)	+0.176 (12)	+0.062 (12)	+0.016 (12)	3
1982.81.....	*r* (λ_{eff} = 6510)	+0.212 (15)	+0.119 (15)	+0.093 (15)	~0.00 (15)	2
1983.83.....	*V*	...	+0.145 (08)	...	+0.010 (06)	4
1986.77.....	*V*	+0.257 (07)	+0.147 (07)	+0.110 (07)	−0.010 (07)	5
	B	+0.303 (08)	+0.162 (08)	+0.141 (08)	−0.039 (10)	
1987.62.....	*V*(FES)	+0.243 (18)	+0.145 (13)	+0.098 (16)	−0.012 (10)	6

[a] REFERENCES.—(1) Eggen 1967; (2) Bradstreet 1985; (3) Davidge & Milone 1984; (4) Poretti 1984; (5) Samec 1989; (6) this paper.

relative to the mean of the two maxima, and the differences in the depths of the minima and the heights of the maxima (max I at 0.25*P*, max II at 0.75*P*). In the cases of Eggen (1967), Poretti (1984), and Davidge & Milone (1984), the data are not available, and these quantities were estimated from enlargements of the published light curves. We noted earlier the odd circumstance that in the light curve plotted by Eggen, the slightly deeper minimum is plotted at 0.5 phase; we took the deeper minimum to be the primary minimum and thus shifted the phases by 0.50. The properties of the light curves are listed in Table 7, along with the filters employed and the epochs of the observations. As can be seen from this table, the largest change is in the relative depth of the shallower minimum (min II). The relative depths and differences between corresponding minima and maxima for the *V* data as well as the unfiltered $\lambda_{eff} \sim 5500$ Å observations are displayed in Figure 15. Because of the definite wavelength dependence apparent in the *B* and *V* light curves of Samec, the red and *B* data are not included in the plot. As shown in this figure, the largest change in the light curve is in the relative depth of the shallower minimum. This plot suggests a possible systematic (nearly linear?) decrease in the relative depth of min II with time of ~0.07–0.08 mag over 20 years. The light curves change from that of Eggen, in which the two minima are of nearly equal depth, to that of Samec, in which the secondary is 0.1 mag shallower. This is a large change, considering that the overall peak-to-peak brightness difference is only ~0.25 mag. There is no evidence of a migrating active region, as is seen in some contact and RS CVn binary systems (see, e.g., Guinan & Giménez 1993, and references therein); major variations seem to be confined to the secondary minimum.

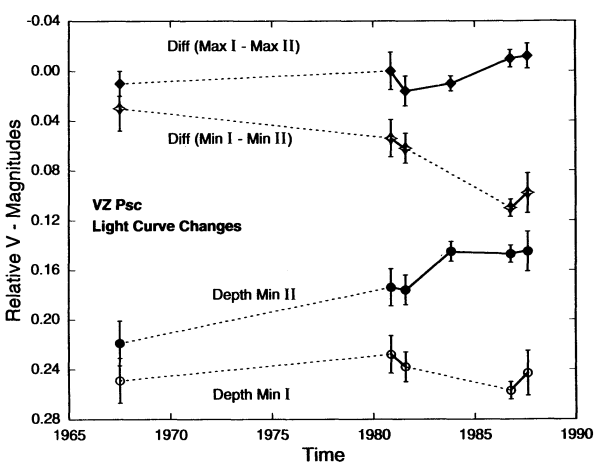

FIG. 15.—Variations among the various *V* light curves of VZ Psc with time

As mentioned in the previous subsection, this change in the depth of the secondary minimum can be explained as a variation in bright regions (hot spots) visible around 0.50 phase. The two models with hot spots (models 3 and 4) suggest that the spots might vary by changing in size (or temperature factor), in longitude, and in number. The systematic decrease seen would be consistent with a portion of a cyclical phenomenon, such as a coherent spot cycle, but such an interpretation is only speculation based upon an apparent systematic trend over 20 years.

A cool spot model, such as the one advanced by Maceroni et al. (1990), appears to be unlikely, because it does not fit with the history of the light-curve variation. In their model, they added cool spots to lower the depth of the deeper minimum (min I), assuming the light curve at min II to be unspotted. But the Eggen (1967) light curve showed min I to be similarly deep, with min II almost as deep. This indicates that the depth of min I does not change but min II does. Maceroni et al. modeled the red light curve of Bradstreet (1985), in which the depth of the two minima differed by 0.09 mag. Thus, to extend their model to the light curve of Eggen would require dark spots to fit both minima, and such an approach based upon the limited light-curve information would not seem to be warranted. If one wants to use cool spots to explain the light curves of VZ Psc, a simpler approach would be to assume that the light curve at primary minimum is unspotted and that cool spots existed at secondary minimum in the Eggen light curve, which had gone away by the time of the newer light curves. Then the newer light curves are unspotted, and the difference in the depths of minimum is intrinsic to the binary system. However, this is the original model which was analyzed prior to the Maceroni et al. study and suffers from the original objections to the HM89 solution, in that it leads to a large temperature difference between the components and a large degree of overcontact. Thus, a model invoking cool spots to fit the unequal minima of the light curves of VZ Psc meets with serious objections when one takes into account both old and new light curves of the system.

5. DISCUSSION AND CONCLUSIONS

Approximate absolute parameters of VZ Psc can be derived from these new velocity- and light-curve solutions. We denote them as approximate because the solution to the light curves is not claimed to be unique, and we have not incorporated the perturbing effects of spots on the velocity-curve solutions. On

TABLE 8

REPRESENTATIVE ABSOLUTE PARAMETERS OF VZ PISCIUM

Element	Component 1	Component 2
Mass ($M_\odot$).....	0.81 (5)	0.65 (4)
Radius ($R_\odot$)	0.78 (2)	0.70 (2)
log T	3.65 (2)	3.61 (3)
log ($L/L_\odot$)	−0.65 (10)	−0.90 (11)
M_{bol} (mag)	6.32 (25)	6.94 (27)
M_V (mag)	6.87 (28)	7.78 (40)
Distance[a] (pc).....	55 (8)	

[a] Assumed reddening of 0.01 mag.

the other hand, we feel that they give a representative model of the system. The approximate or representative absolute parameters are listed in Table 8. They are based upon the light curve solution model 4, listed in Table 6, and the velocity-curve solution from Table 5 which includes the light-curve model without spots. For a representative radius of the stars, we list the radii of spherical stars of the same volume, as tabulated by Mochnacki (1984). The luminosity is determined from the temperatures and surface areas of the stars. We have assumed an uncertainty in the temperatures of 250 K. In computing the luminosity, we have neglected the effect of the spots. We have adopted solar values of $T_{eff} = 5780$ K and $M_{bol} = 4.69$, and bolometric corrections for the components using the value of Popper (1980). Using the observed V magnitude at maximum light of 10.2 and a reddening of 0.01 (Rucinski & Kaluzny 1981; Bradstreet 1985; Rucinski 1983), we calculate a distance to the system of 55 pc. The system is close enough for a parallax to be measured, but one has not been published; a parallax will provide a useful constraint on the model of this system. The calculated masses of the components are now in agreement with the masses of K0–K5 dwarfs as tabulated by Popper (1980), and the radii agree with those of early to mid-K dwarfs.

Thus, the derived parameters from our new solutions are physically consistent with observations of cool, low-mass stars (as are those of Maceroni et al. 1990). They do not have the unusually (and unrealistically) large value of mass found from the solution of Hrivnak & Milone (1989). This is because the new models with spots possess a higher inclination and do not need a large temperature difference between components to explain the difference in the depths of the minima. The advantages of these new solutions over those of Maceroni et al. are that (a) they incorporate an improved value of the mass ratio, (b) they are better constrained because they are based upon fits to multicolor light curves, and (c) they include solutions with hot spots, which agree better with all of the spectroscopic and photometric data than does a cool spot model.

One of the outstanding properties of VZ Psc is its large space motion. This value has not been changed significantly by this study from that of Hrivnak & Milone (1989). The space motion is greater than 100 km s^{-1} and indicates that the system is composed of old disk (or even Population II) objects. The high mass ratio suggests that the two stars are presently evolving into contact and have not experienced significant mass exchange. The progenitor would have likely been a pair of K dwarfs with an initial orbital period of 4–5 days (see Guinant & Bradstreet 1988), similar to the BY Draconis–type binaries.

We have found the system to display strong emission lines due to Mg II (2800 Å), Ca II (3933, 3968 Å), and Hα; all of these are indicators of chromospheric activity. The Mg II and Ca II emissions, when normalized to the emitted stellar flux, do not appear to be phase dependent. However, the chromospheric activity does vary over intervals of several hours (Mg II) and night to night (Ca II). Chromospheric studies of only a few other contact binaries have been published. Eaton (1986a) found a slight phase dependence in the normalized Mg II emission of SW Lac, in the sense that the emission was slightly greater at the secondary minimum, when the less massive component was in front. Little phase or annual variations in Mg II emission is found for VW Cep from 30 *IUE* spectra made over three observing seasons: 1979, 1981, and 1983 (Eaton 1985). For V566 Oph, an earlier spectral type system, no variation was seen in the normalized Mg II emission at more than the 10% level (Eaton 1986b). Rucinski, Vilhu, & Whelan (1985) examined the Lyα emission of W UMa and found no phase dependence in the normalized flux. Vilhu & Rucinski (1985) found no phase dependence in the normalized Mg II emission from XY Leo; however this system is complicated by the discovery of a BY Draconis–type binary forming a quadruple system with XY Leo (Barden 1987). A study of 44 ι Boo suggested some phase dependence in the normalized C IV flux, although the accuracy of the measurements is low (Rucinski & Vilhu 1983). Thus, in general, these studies have found little or no phase dependence in the chromospheric activity in contact binaries. For VZ Psc, we seem to see a base level in the Mg II emission with no phase dependence, and then an increase by as much as 50% which can last for 1–2 hr. This increase may be caused by either flaring in the system or an increase in the emission of an active region which moves into and out of view.

The Ca II emission can be resolved into separate components from each of the two stars. The strength of the Ca II feature is found to be greater from component 2, the less massive star. We used this fact and the Ca II velocity curve to suggest that the model with hot spots on the inner hemisphere of component 2 was the most likely. Note that, while we have fitted the light curves with two circular spots having the same latitude and on the same side of the star, the light curves might be fitted as well by one region elongated in longitude. It would be difficult to distinguish between two close spots and an elongated region on the basis of the modeling, and perhaps an elongated bright region is more appealing physically. However, we have not tried to model this.

We can try to physically understand how such hot spots or regions might arise. In semidetached systems, hot spots can arise from the impact of a stream of material passing from the component which fills its lobe through the inner Lagrangian point and onto the detached mass gainer. The impact produces kinetic heating of the mass-gaining star's photosphere. Some Algol-type binaries, including β Per itself, show strong evidence in the ultraviolet for heated regions in the inner hemisphere of the mass-gaining star, resulting from the impact of a gas stream (see, e.g., Guinan 1990, and references therein). The long-lasting asymmetries in the light curves of the near-contact eclipsing binary V361 Lyr have recently been modeled with a hot spot, most likely produced from the impact of a gas stream (Kaluzny 1990; Bradstreet et al. 1993). Episodes of mass transfer could produce variabile heating of the inner hemisphere of the gainer. Our best model, that with hot spots on the inner hemisphere of component 2 (model 4), fits this configuration; component 1 fills its Roche lobe, and component 2 is (slightly) detached. Even in this case, one encounters the problem that one hot spot would be expected where the stream impacted, but not two spots, as found from the light-curve models

(although perhaps an elongated region). The standard theoretical picture of the evolution of contact binaries has the massive component transferring mass and energy once it has filled its Roche lobe to the detached, less massive component, until the later has responded by expanding to also fill its Roche lobe. Then in the contact configuration, the direction of mass transfer is from the less to the more massive component. (See Smith 1984 for a general review of evolution in W UMa binary systems.) VZ Psc can be compared with this theoretical picture. As stated above, in VZ Psc it is the slightly detached, less massive component which has the hot spots on its inner hemisphere. Perhaps this arises as mass is transferred from the more massive companion, which fills its Roche lobe. The high mass ratio of VZ Psc suggests that it may be presently evolving into a contact configuration, since the above evolutionary picture indicates evolution toward smaller mass ratios for systems when they come into contact. Thus, one may still be seeing the effects of the mass transfer into contact for this system.

Even if the system were not slightly detached but in marginal contact, it might still be possible to explain the hot spots. Hot spots (bright regions) have been observed on both single and binary stars. They can arise from magnetic dynamo effects and may be related to white-light faculae observed on the Sun. Bright light regions have been observed on some detached RS CVn binary systems (see, e.g., Dorren & Guinan 1990). Whether such mechanisms as these could produce relatively stationary spots seen to occur only around the inner hemisphere of one of the components is not apparent. Perhaps it is the case that mass and energy transfer in a contact binary system lead to a heating and brightening of the neck region and inner hemisphere of one of the components, and that we are seeing this in the inner hemisphere of the less massive star in VZ Psc. Kaluzny, in a series of papers studying several "contact binaries with components in poor thermal contact," found that to fit the light curves required regions of higher surface brightness near the neck region of the cooler component (Kaluzny 1986, and references therein). This is exactly what we have found here. Kaluzny modeled this by allowing the bolometric albedo of the cooler component to have a physically unrealistic value of greater than 1.00. This was the same tactic used by Lucy & Wilson (1979) to model two other contact binaries with large differences in the depths of minimum. There is also evidence from high-resolution ultraviolet spectroscopy of excess Mg II emission from the neck region of the short-period contact binary VW Cep (Bradstreet & Guinan 1990) which could indicate heating there.

It may well be the case that, in addition to the large spots discussed above, small additional spots are widely distributed on both components. We note that the intrinsic light-curve variation is not confined to the secondary minimum. Light-curve variations in the phase interval 0.1–0.4 were observed by Bradstreet (1985) over an interval of 35 days, with a peak-to-peak variation of 0.06 mag at phase 0.25. Also, strong Ca II emission associated with active regions on the stars was observed at all phases.

In addition to its high mass ratio, VZ Psc is unusual among W UMa binary systems in that it is viewed at a low inclination angle (48°) and therefore undergoes only very shallow eclipses. (Most of the light variation is caused by the oblate shapes of the stars.) The low inclination of the system, as determined from the light curves, makes it difficult to extract precise information from its low-amplitude light curves. On the other hand, VZ Psc does offer an important opportunity to view directly the inner hemispheres of both stars of a W UMa system, since these regions are not significantly eclipsed during the orbital conjunctions, as is the case in almost all other W UMa systems. For this reason, the presence of a bright region on the inner hemisphere of the less massive component and changes in the bright region with time can be clearly documented for VZ Psc, while they would most likely be unnoticed in other, higher inclination, W UMa systems.

VZ Psc remains an important, but difficult, binary system that deserves further investigation. The present study has advanced our understanding of the system, but more remains to be learned and confirmed. Reasonable models of the system require spots to fit the light curves, and comparison of the light curves from different epochs indicate that these spots vary. The combination of spectroscopic and photometric data has permitted us to chose among the several spot models in favor of the one with hot spots on the less massive component. A new photometric study is urgently needed to determine the long-term evolution of the light curves with time. The last published light curve was obtained in 1986. *BV* (or even better, *UBVRI* and perhaps *JHK*) light curves would possibly give one new insight in choosing among the models of the system and allow one to determine the source of the long-term light variations. We discussed the necessity of obtaining simultaneous light and velocity curves to allow the effects of the light distribution, including spots, to be modeled consistently for both the light and velocity curve solutions. In addition, a high signal-to-noise ratio, high-resolution spectroscopic study would be very helpful to determine unambiguously the distribution of surface features on the components using the line-broadening technique. However, because of the shallowness of the absorption features on these rapidly rotating stars and the relative faintness of the system for high signal-to-noise ratio observations, it would require a very large aperture telescope, 4 m class or larger. The acquisition of a trigonometric parallax would permit a tighter constraint on the parameters of the system and perhaps will be forthcoming from the HIPPARCOS mission. Thus, while additional observations would be helpful in the understanding of this system, the results of this study clearly demonstrate the value of having a variety of complementary data in trying to model a low-inclination, intrinsically variable system such as VZ Psc.

We are grateful to G. Hill for making available his spectroscopic reduction and spectroscopic binary orbit programs, to R. E. Wilson for making available his synthetic light-curve programs, and to B. W. Bopp for the Hα spectrum of VZ Psc. The comments of the anonymous referee about the light-curve modeling were helpful and led to improved light-curve solutions. Undergraduate C. A. Goehring assisted in the reduction of the ground-based spectra. D. Duncan and P. Nord kindly assisted with preparing the figures. The assistance of the staff of the *IUE* and the hospitality at the Dominion Astrophysical Observatory were much appreciated. This research was supported by grants to B. J. H. from NASA (NAG 5-964) and the National Science Foundation (AST-8815897) and to E. F. G. from NASA (NAG 5-2160); these are all gratefully acknowledged.

REFERENCES

Al-Naimiy, H. M. K. 1978, Ap&SS, 53, 181
Barden, S. C. 1985, ApJ, 295, 162
———. 1987, ApJ, 317, 333
Barone, F., Milano, L., Russo, G., & Sarna, M. J. 1989, Ap&SS, 159, 67
Binnendijk, L. 1970, Vistas Astron., 12, 217
———. 1984, PASP, 96, 646
Bopp, B. W., et al. 1985, ApJ, 297, 691
Bradstreet, D. H. 1985, ApJS, 58, 413
———. 1993, in Light Curve Modeling of Eclipsing Binary Stars, ed. E. F. Milone (New York: Springer-Verlag), 151
Bradstreet, D. H., & Guinan, E. F. 1990, in Active Close Binaries, ed. C. Ibanoglu (Dordrecht: Kluwer), 467
Bradstreet, D. H., Nations, H. L., Guinan, E. F., & Laurenzano, J. 1993, BAAS, 26, 793
Davidge, T. J., & Milone, E. F. 1984, Inf. Bull. Variable Stars, 2639
Dorren, J. D., & Guinan, E. F. 1990, ApJ, 348, 703
Eaton, J. A. 1985, Inf. Bull. Variable Stars, 2711
———. 1986a, Acta Astron., 36, 79
———. 1986b, Acta Astron., 36, 275
Eggen, O. J. 1967, ApJ, 150, L111
Flannery, B. P. 1976, ApJ, 205, 217
Fouts, G. 1987, PASP, 99, 986
Guinan, E. F. 1990, in Evolution in Astrophysics: IUE Astronomy in the Era of New Space Missions, ed. E. J. Rolfe (ESA SP-310), 73
Guinan, E. F., & Bradstreet, D. H. 1988, in Formation and Evolution of Low Mass Stars, ed. A. K. Dupree & M. T. Lago (Dordrecht: Kluwer), 345
Guinan, E. F., & Giménez, A. 1993, in The Realm of Interacting Binary Stars, ed. J. Sahade, G. E. McCluskey, Jr., & Y. Kondo (Dordrecht: Kluwer), 51
Hill, G. 1982, Publ. Dom. Astrophys. Obs. Victoria, 16, 59
Hill, G., & Fisher, W. A. 1986, Publ. Dom. Astrophys. Obs. Victoria, 16, 159
Hill, G., Fisher, W. A., & Poeckert, R. 1982, Publ. Dom. Astrophys. Obs. Victoria, 16, 43
Hrivnak, B. J. 1988, ApJ, 335, 319
———. 1989, ApJ, 340, 458
———. 1993, in New Frontiers in Binary Star Research, ed. K. C. Leung & I.-S. Nha (ASP Conf. Ser. 38), 269
Hrivnak, B. J., & Milone, E. F. 1989, AJ, 97, 532 (HM89)
Imhoff, C. L. & Wasatonic, R. 1986, NASA *IUE* Newsletter, 29, 45
Johnson, H. L. 1966, ARA&A, 4, 193
Kaluzny, J. 1986, PASP, 98, 662
———. 1990, AJ, 99, 1207
Lee, S. G. 1984, AJ, 89, 702
Linnell, A. P. 1982, in 2d Cambridge Workshop on Cool Stars, Stellar Systems and the Sun, ed. M. S. Giampapa & L. Golub (New York: Springer), 65
Lucy, L. B. 1976, ApJ, 205, 208
Lucy, L. B., & Wilson, R. E. 1979, ApJ, 231, 502
Maceroni, C., Van Hamme, W., & van't Veer, F. 1990, A&A, 234, 177
Milone, E. F., Frey, D. J. I., Davidge, T. J., & Hrivnak, B. J. 1985, BAAS, 17, 754
Milone, E. F., Hrivnak, B. J., & Fisher, W. A. 1985, AJ, 90, 354
Mochnacki, S. W. 1981, ApJ, 245, 650
———. 1984, ApJS, 55, 551
Popper, D. M. 1980, ARA&A, 18, 115
Poretti, E. 1984, Inf. Bull. Variable Stars, 2487
Rodono, M., et al. 1986, A&A, 165, 135
Rucinski, S. M. 1983, A&A, 127, 84
———. 1985, MNRAS, 215, 615
Rucinski, S. M., & Kaluzny, J. 1981, Acta Astron., 31, 409
Rucinski, S. M., & Vilhu, O. 1983, MNRAS, 202, 1221
Rucinski, S. M., Vilhu, O., & Whelan, J. A. 1985, A&A, 143, 153
Rucinski, S. M., Whelan, J. A., & Worden, S. P. 1977, PASP, 89, 684
Samec, R. G. 1989, PASP, 101, 661
Smith, R. C. 1984, QJRAS, 25, 405
Stephenson, C. B. 1986, AJ, 92, 139
Vilhu, O. 1982, A&A, 109, 17
Vilhu, O., & Rucinski, S. M. 1985, Acta Astron., 35, 29
Vilhu, O., & Walter, F. M. 1987, ApJ, 321, 958
Wilson, R. E. 1979, ApJ, 234, 1054
———. 1992, Documentation of Eclipsing Binary Computer Model (Gainsville: Univ. Florida)
Wilson, R. E., & Devinney, E. J. 1971, ApJ, 166, 605
Wolff, S. C., Wallerstein, G., & Sandage, A. R. 1965, PASP, 77, 370
Zhai, D., & Lu, W. 1989, Chinese Astron. Astrophys., 13, 350